Developments of the wideband spectropolarimeter of the Domeless Solar Telescope at Hida Observatory

Tetsu Anan[a], Kiyoshi Ichimoto[a], Akihito Oi[a], Goichi Kimura[a], Yoshikazu Nakatani[a], and Satoru Ueno[a]

[a]Kwasan and Hida Observatories, Gifu 506-1314, Japan

ABSTRACT

We developed a new universal spectropolarimeter on the Domeless Solar Telescope at Hida Observatory to realize precise spectropolarimetric observations in a wide range of wavelength in visible and near infrared. The system aims to open a new window of plasma diagnostics by using Zeeman effect, Hanle effect, Stark effect, and impact polarization to measure the external magnetic field, electric field, and anisotropies in atomic excitation in solar atmosphere. The polarimeter consists of a 60 cm aperture vacuum telescope, a high dispersion vacuum spectrograph, polarization modulator and analyser composed of a continuously rotating waveplate whose retardation is constant in 400 - 1100 nm and Wallaston prisms located closely behind the focus of the telescope, and a fast and high sensitive CCD camera or a infrared camera. The duration for this polarimeter's achieving photometric accuracy of 10^{-3} is 30 - 60 s. Instrumental polarization of the telescope is calibrated by using a remotely controllable turret accommodating linear polarizer attached at the entrance window of the telescope to induce well known polarized light into the telescope. Thus a Mueller matrix model of the telescope is established to compensate the instrumental polarization included in observed data within the required accuracy.

Keywords: Solar observation, Spectropolarimeter, High sensitivity, Wide wavelength range, Ground-based telescope, Instrumental polarization

1. INTRODUCTION

Since Hale[1] discovered existence of a strong magnetic field in sunspot by observing Zeeman effect in circular polarization spectra, the Zeeman effect has been the primary mean to diagnose the magnetic fields in solar photosphere and it is revealed that the magnetic field is the key physical ingredient behind the solar activity and various solar phenomena. In contrast to the photosphere, it is difficult to diagnose magnetic fields in the solar chromosphere, i.e., the boundary region between the solar corona and the photosphere, in which the dominant force changes from hydrodynamic pressure to magnetic forces. There are two reasons why it is difficult to diagnose the magnetic fields in the chromosphere. First, the polarization signal produced by the Zeeman effect scales with the ratio of the Zeeman splitting and the Doppler width, and the ratio turns out to be very small for chromospheric lines. Second, the interpretation of the polarization in chromospheric lines is complicated, because polarization mechanism in the chromosphere is not only the Zeeman effect but also, for example, coherent scattering modified with the Hanle effect.

Recently, the developments of polarimeter enable us to detect the weak polarization in chromospheric lines (e.g. Zurich Imaging Stokes Polarimeter II[2] , Tenerife Infrared Polarimeter II[3] , and Facility Infrared Spectropolarimeter[4]). If the polarization sensitivity of 10^{-4} is achieved, we can detect the Hanle effect, a modification of the coherent scattering polarization by magnetic field. The Hanle effect provides us an opportunity to diagnose small scale turbulent or tangled magnetic fields[5] and weak magnetic fields that cannot be reached with the Zeeman effect. On the other hand, some polarization line profiles produced by coherent scattering, ex. Na I D_1, are not understood with the current quantum mechanical description[6] and atomic polarization of metastable level are still enigmatic[7] .

Further author information: (Send correspondence to Tetsu Anan)
Tetsu Anan: E-mail: anan@kwasan.kyoto-u.ac.jp, Telephone: +81 (0)80 3091 3185
Kiyoshi Ichimoto: E-mail: ichimoto@kwasan.kyoto-u.ac.jp, Telephone: +81 (0)578 86 2118

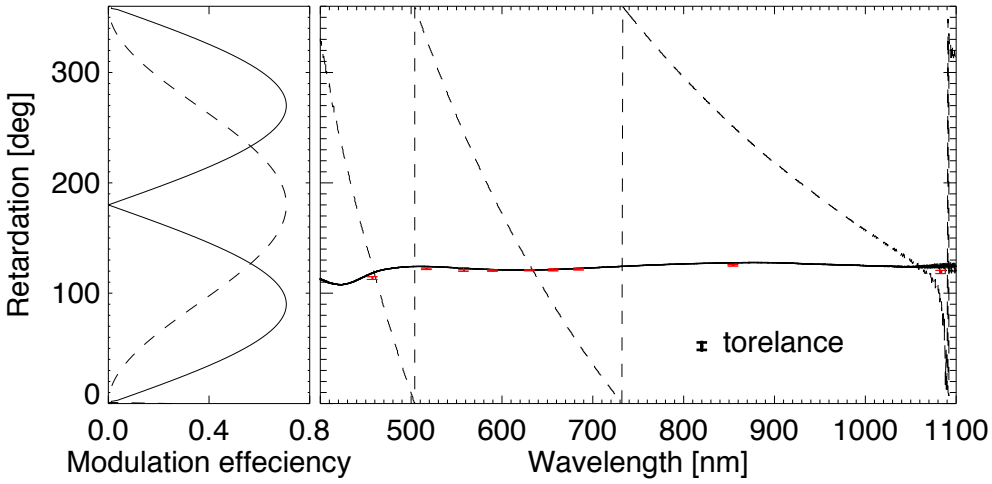

Figure 1. Retardation of waveplates used as modulator (right) and modulation efficiency[13] as function of a retardation (left). In the left panel, solid line and dashed lines indicate the modulation efficiency for circular and linear polarizations, respectively. In the right panel, Black solid line and dashed lines are retardation of the APSAW and the quartz waveplate measured by using a photopolarimetric measurement system of Mueller matrix with dual rotating waveplates[14] , respectively. Red symbols are the retardation of APSAW derived from intensity modulation observed when complete linear polarized light incident on our modulator with analyzer.

The Stark effect and anisotropic collisional excitation (impact) of atoms also produce a polarization of spectral lines of the order of 10^{-3}. The Stalk effect would enable us to diagnose an electric field induced, for example, when neutral atoms move across a magnetic field[8] , and the impact polarization would enable us to diagnose anisotropy of velocity distribution of particles by heat conduction or accelerated high-energy particles which penetrate into the chromosphere[9] . However studies incorporating these effects are quite limited so fer.

In order to utilise these polarization mechanisms to open a new window of plasma diagnostics, we developed a system which enable us to make precise spectro-polarimetric observations in a photometric accuracy of 10^{-3}- 10^{-4} for wide wavelength range in visible and near infrared. The requirements on the accuracy and the sensitivity of the polarization calibration to achieve our aim are established in the same manner as Ichimoto et al.[10] , but with different parameters; i.e., the statistical noise, the allowable scale error, maximum incoming linear polarization, and maximum incoming circular polarization to be 10^{-4}, 0.05, 0.02, and 0.02, respectively. In this paper, an axis which rotate 45° from positive Q in counterclockwise looking at the source is defined as positive U, and the right circular polarization, when an electric vector rotates clockwise looking at the source is defined as positive V. In the following sections, we describe the detail of new developed polarimeter (Section 2), calibration of instrumental polarization of the telescope (Section 3), and finally discuss and summarize our developments (Section 4).

2. NEW POLARIMETER

The new polarimeter is a successor of formerly developed polarimeter on the Domeless Solar Telescope (DST) at Hida observatory, which was aimed to measure the vector magnetic fields in the photosphere[11] . The system consists of a 60 cm aperture vacuum telescope, a high dispersion vertical vacuum spectrograph, polarization modulator and analyser composed of a rotating waveplate and Wallaston prisms located closely behind the focus of the telescope, and a CCD camera or infrared camera. Details of DST will be described in section 3. The vacuum spectrograph is equipped with a grating of $306 \times 408\,\mathrm{mm}^2$ ruled area, of 632 grooves/mm, and Blaze angle is 56°[12] . The length of the spectrograph slit is 20 mm that corresponds to the angular scale of 128 arcsec on the sun. Entire spectrograph including the entrance slit, rotating waveplate and polarization analyzer is rotatable about the vertical optical axis of the DST.

Observed intensity of spectrum $I_{\pm}^{obs}$ in orthogonal polarizations separated by the polarization analyzer can be written with the following forms as functions of the rotation angle of the waveplate (θ_i) at the ith exposure start time.

$$I_{\pm}^{obs}(\theta_i) = (1-r)^2\, R_{\pm} \left\{ \left(C_1 \pm C_2 \cos 2\,\theta_i'\right) I^{in} \pm \left(C_3 \cos 4\,\theta_i' + C_4\right) Q^{in} \pm C_3 \sin 4\,\theta_i'\; U^{in} \pm C_5 \sin 2\,\theta_i'\; V^{in} \right\}$$

$$\begin{aligned}
C_1 &= \frac{\epsilon}{2} \\
C_2 &= r^2\, \frac{T}{2\pi} \sin\left(\frac{2\pi\epsilon}{T}\right) \sin\left(\frac{4\pi dn}{\lambda}\right) \sin\delta \\
C_3 &= \frac{T}{8\pi} \sin\left(\frac{4\pi\epsilon}{T}\right) \frac{1-\cos\delta}{2} \\
C_4 &= \frac{\epsilon}{2}\, \frac{1+\cos\delta}{2} \\
C_5 &= \frac{T}{4\pi} \sin\left(\frac{2\pi\epsilon}{T}\right) \sin\delta \\
\theta_i' &= \theta_i + \pi\frac{\epsilon}{T} + \alpha,
\end{aligned}$$

where $\pm$ indicate each light of dual orthogonal beam, $(I^{in}, Q^{in}, U^{in}, V^{in})$ are the Stokes vector of the incident light, λ is the wavelength, $R_{\pm}$ is transmittance of spectrograph for each beam, ϵ is the exposure time, and α is the angle between the fast axis of the waveplate and the direcion of the Wallaston prism when the first exposure is triggered. T, δ, r, d, and n is the rotation period, the retardation, the surface reflectivity, the thickness, and the refractive index of the waveplate, respectively. On the focal plane of DST, we define an axis of Wollaston prism that is perpendicular to the spectrograph slit as positive Q. $\mathbf{S^{in}} \equiv (I^{in}, Q^{in}, U^{in}, V^{in})$ and $\mathbf{\Delta I^{obs}} \equiv \left(\frac{I_+^{obs}(\theta_1) - I_-^{obs}(\theta_1) R_+/R_-}{2}, \ldots, \frac{I_+^{obs}(\theta_n) - I_-^{obs}(\theta_n) R_+/R_-}{2}\right)$ are connected with a $4 \times n$ 'modulation matrix' $\mathbf{M}$.

$$\begin{aligned}
\Delta I_i^{obs} &= \sum_{j=1}^{4} M_{ij}\, S_j^{in} \\
&= (1-r)^2 R_+ \left\{ C_2 \cos 2\theta_i'\; I^{in} + \left(C_3 \cos 4\theta_i' + C_4\right) Q^{in} + C_3 \sin 4\theta_i'\; U^{in} + C_5 \sin 2\theta_i'\; V^{in} \right\},
\end{aligned}$$

The inverse matrix $\mathbf{W}$ of the modulation matrix $\mathbf{M}$ can be obtained with the following form, and we are able to get the input Stokes vector as the product of $\mathbf{W}$ and $\mathbf{\Delta I^{obs}}$,

$$\mathbf{W} = (\mathbf{M}^T\mathbf{M})^{-1}\mathbf{M}^T,$$

where the superscript T denotes the transpose of the matrix. Our tolerance of the retardation, the rotation angle, and the stability of exposure time are determined in the same manner as Ichimoto et al.[10] and are 3.4°, 0.07°, and 100 μs, respectively.

Figure 1 shows the modulation efficiencies for Stokes-Q, U, and V as a function of the retardation of the waveplate and the measured retardation of our waveplates as a function of wavelength. In the former system[11], the wavelength range of high modulation efficiency is limited with a 163 μm thick quartz waveplate and it took 30 s to take 16 images with a slow camera and step-wise motion of the rotating waveplate. On the new system, the polarimeter is equipped with a fast and high sensitive CCD camera (Procilica GE1650, manufactured by Allied Vision Technologies Co.), a infrared camera (XEVA-1.7-640, manufactured by Xenics Co.), Super-Achromatic True Zero-Order Waveplates (APSAW, manufactured by Astropribor Co.), and a continuously rotating waveplate equipped with an origin sensor on it. APSAW have high modulation efficiency in a wavelength range from 400 nm to 1100 nm. Wide wavelength range is covered by using one of the CCD camera and the infrared camera. The origin sensor produces a trigger for the camera to start a sequence of exposures for both orthogonal polarization spectra split by the Wallaston prisms. Maximum frame rate at full resolution is about 30 frames per second.

Thus the new system enable us to take spectral images in both orthogonal polarizations simultaneously with a frame rate of ∼30 Hz for wide range of wavelength while the waveplate rotates continuously in a rate of 1 Hz.

It takes ∼30 s and ∼60 s to achieve photon random noise to 10^{-3} in visible and near infrared in typical setup with the spatial sampling of 0.4 arcsec and spectral sampling of 4 pm in visible (589 nm) and of 0.6 arcsec and spectral sampling of 3 pm in infrared (1083 nm), respectively, while it takes more than ∼150 s by the former system in visible to achieve the same noise level. The accuracy of the rotation angle and the retardation of waveplate are verified within our tolerance. The accuracy of the exposure time of camera is 1 μs within our tolerance. In typical observation, we take 16 - 20 exposures in one rotation of the waveplate, and demodulation is made by extracting the 2θ, $\sin 4\theta$ and $\cos 4\theta$ components from the observed intensity modulation for Stokes-V, Q, and U, respectively. Although interference fringes produced by internal reflection of the waveplate modulate the intensity in similar way with the Stokes-V, the fringes do not effect on the measurement of Stokes vector, since its modulation is 90° apart in phase from the Stokes-V signal. Two orthogonaly polarized spectra are aligned and combined to eliminate the intensity variations caused by seeing and guiding error during the integration.

3. INSTRUMENTAL POLARIZATION OF DST

The DST is a 60 cm Newton-Gregorian type telescope on alt-azimuth mount[15,12]. Figure 2 shows the ray path along the DST and its optical components. The solar ray goes through an entrance window and an entrance pupil with an aperture of 600 mm before it reaches a primary mirror that has 633 mm of diameter. The primary mirror with a focal length of 3.150 m (F5.1) produces a 3 cm solar image on the elevation axis of the tube, which is 21.5 m high from the ground level. The conversing light reflected by the Newton mirror passes through a central hole of the Coude mirror and reaches to the Gregory secondary mirror with a diameter of 452 mm. Then after reflected by the Coude mirror and transmitting the exit-window, the Gregory secondary mirror forms a 300 mm solar image at the observing table of the spectrograph. The space between the entrance-window and the exit-window is kept vacuum down to 2 mmHg to avoid air turbulence.

The entrance and exit windows are 40 mm in thickness and made of BK7 and UBK7, respectively. They are also coated with MgF_2 to increase the UV transmission. All mirrors are aluminized and made of Zerodur. In addition to being aluminized, the Newton, secondary, and Coude mirror are also overcoated with Zeiss-H08 coating to increase the reflectivity.

It is important to calibrate the instrumental polarization of the DST to realize accurate polarization measurement, because the two flat oblique mirrors (Newton mirror and Coude mirror) of the DST produce a non-negligible instrumental polariztion. The telescope Muellar matrix model we consider is almost the same as that of Makita et al.[16], Kiyohara et al.[11], and Hanaoka[17]. Their model can represent the instrumental polarization with an accuracy of 0.009 at 630 nm[17]. Since the details of the coating of mirrors are unknown, we set thier properties as unknown parameters of the model for wide range of wavelength and obtained them by fitting the model with observation data obtained by introducing known polarized light into the telescope.

3.1 DST polarization model

The propagation of the polarization through the DST is described by the product of the Mueller matrices of individual optical elements in proper order including rotation matrix of the coordinate. Each Mueller matrix of the optical elements and rotation matrices of coordinates are described as bellows.

Rotation of coordinate is written as

$$\mathbf{R}(\theta) = \begin{pmatrix} 1 & 0 & 0 & 0 \\ 0 & \cos 2\theta & \sin 2\theta & 0 \\ 0 & -\sin 2\theta & \cos 2\theta & 0 \\ 0 & 0 & 0 & 1 \end{pmatrix},$$

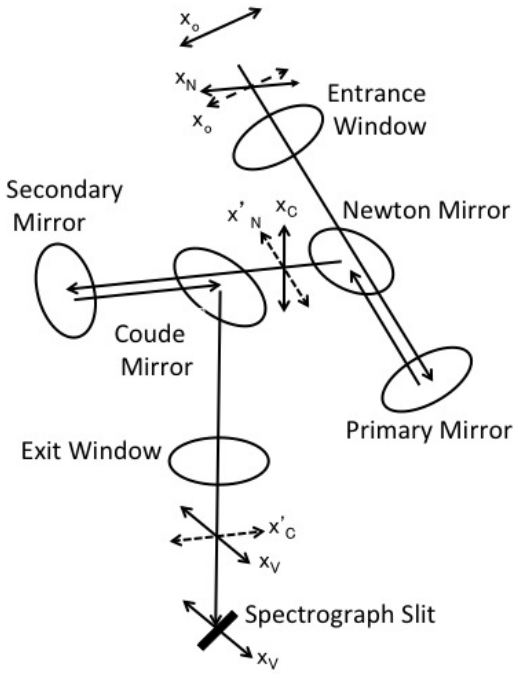

Figure 2. The ray path along the DST. The arrows x_N (x'_N) and x_C (x'_C) are included in the incident and reflection plane of the Newton and Coude mirrors, respectively. The arrow x_o indicates the reference coordinate of the Stokes vector of the light entering into the DST. The arrow x_V is the direction of analyzer in perpendicular to the slit of the vertical spectrograph.

where a plus sign of the rotation angle θ indicates a counterclockwise rotation looking at the light coming to. Each 4 mirrors in the DST is described as the same form

$$\mathbf{M} = \frac{1}{1+p}\begin{pmatrix} 1 & p & 0 & 0 \\ p & 1 & 0 & 0 \\ 0 & 0 & -\sqrt{1-p^2}\cos\tau & -\sqrt{1-p^2}\sin\tau \\ 0 & 0 & \sqrt{1-p^2}\sin\tau & -\sqrt{1-p^2}\cos\tau \end{pmatrix},$$

where p and τ are the difference of reflectivity and phase between the polarizations which are parallel and perpendicular to the plane of incidence, respectively. The axis of positive Q is defined as included in the plane defined by incident and reflected rays at each surface. Mechanical stress on the two windows could make them act as a weak linear retarder[18] and the Mueller matrix referred to the fast axis of the window is represented as

$$\mathbf{D} = \begin{pmatrix} 1 & 0 & 0 & 0 \\ 0 & 1 & 0 & 0 \\ 0 & 0 & \cos\delta & \sin\delta \\ 0 & 0 & -\sin\delta & \cos\delta \end{pmatrix},$$

where δ is the retardation of the window.

In our polarimetric system, direction of positive Q of the incident light is defined as the east-west direction (x_o) on the celestial sphere. The Mueller matrix of DST, $\mathbf{T_{DST}}$, is written as

$$\mathbf{T_{DST}} = \mathbf{S}\ \mathbf{R}(-\theta_{ex})\mathbf{D_{ex}}\mathbf{R}(\theta_{ex})\ \mathbf{R}(-\theta_C)\mathbf{M_C}\mathbf{R}(\theta_C)\ \mathbf{R}(-\theta_G)\mathbf{M_G}\mathbf{R}(\theta_G)$$

$$\mathbf{R}(-\theta_N)\mathbf{M_N}\mathbf{R}(\theta_N)\ \mathbf{R}(-\theta_P)\mathbf{M_P}\mathbf{R}(\theta_P)\ \mathbf{R}(-\theta_{en})\mathbf{D_{en}}\mathbf{R}(\theta_{en}),$$

where $\mathbf{D_{ex}}$ and $\mathbf{D_{en}}$ are the Mueller matrices of exit and entrance window, respectively. $\mathbf{M_C}$, $\mathbf{M_G}$, $\mathbf{M_N}$, and $\mathbf{M_P}$ are the Mueller matrices of Coude, Gregorian secondary, Newton, and Primary mirror, respectively. $\mathbf{R}$ is the rotation matrix and θ_{en}, θ_P, θ_N, θ_G, θ_C, and θ_{ex} are the angle between positive Q of the incident light and the axis of the entrance window, the primary mirror, the Newton mirror, the Gregorian secondary mirror, the Coude mirror, and the exit window, respectively. In addtion to the DST model described in Makita et al.[16] , we consider an effect of unpolarized stray light in the telescope which is written as a fictitious Mueller matrix

$$\mathbf{S} = \begin{pmatrix} 1+s & 0 & 0 & 0 \\ 0 & 1 & 0 & 0 \\ 0 & 0 & 1 & 0 \\ 0 & 0 & 0 & 1 \end{pmatrix},$$

where s is the fraction of stray light in the intensity.

Primary mirror, Gregorian secondary mirror and two windous are regarded as ideal ones in polarization, because they are symmetry with respect to the optical axis and the incident angle to them are very small. Thus we can rewrite the Mueller matrix of DST

$$\mathbf{T'_{DST}} = \mathbf{S}\,\mathbf{M_C}\mathbf{M_G}\mathbf{R}(\phi_\mathbf{C})\mathbf{M_N}\mathbf{M_P}\mathbf{R}(\phi_\mathbf{N}),$$

where $\mathbf{M_G}$ and $\mathbf{M_P}$ are as the follows.

$$\mathbf{M_G} = \mathbf{M_P} = \begin{pmatrix} 1 & 0 & 0 & 0 \\ 0 & 1 & 0 & 0 \\ 0 & 0 & -1 & 0 \\ 0 & 0 & 0 & -1 \end{pmatrix},$$

ϕ_N is the angle between x_o and x_N, and ϕ_C is the angle between x'_N and x_C, where x_N (x'_N) and x_C (x'_C) are axes included in the incident and reflection plane of the Newton and Coude mirrors, respectively (see Fig. 2).

The axis x'_C which is coordinate axis of the Coude mirror does not coincide with that of analyzer (x_V). The Mueller matrix of entire telescope, $\mathbf{T_V}$, thus include a rotating matrix of the angle between x'_C and x_V

$$\mathbf{T_V} = \mathbf{R}(\phi_\mathbf{V})\mathbf{S}\,\mathbf{M_C}\mathbf{M_G}\mathbf{R}(\phi_\mathbf{C})\mathbf{M_N}\mathbf{M_P}\mathbf{R}(\phi_\mathbf{N}). \quad (1)$$

where ϕ_V is the angle between x'_C and x_V. The angles in Equation (1) can be written using the hour angle θ_{HA} and the zenith distance θ_{ZD} of the sun as follows,

$$\begin{aligned} \phi_N &= \theta_{ZA} \\ \phi_C &= \mp\theta_{ZD} \\ \phi_V &= \pm\theta_{ZD} - \theta_{ZA} + \theta_i \\ \theta_{ZA} &= \arcsin\Big(\frac{\cos\theta_{lat}\sin\theta_{HA}}{\sin\theta_{ZD}}\Big), \end{aligned}$$

where θ_{lat} is the latitude of Hida Observatory and the upper and the lower signs of $\pm$ or $\mp$ are for when the telescope tube is set westward and eastward to the rotation axis of the azimuth, respectively. Since the configuration and the Mueller matrix of DST change as the hour angle and the zenith distance of the sun, we need to record these angles during observation.

To calibrate instrumental polarization of DST, we consider only the effect of two flat oblique mirrors in the model of DST. Thus the model has five unknown parameters (p_N, τ_N, p_C, τ_C, s) where p_N and τ_N are p and τ of the Newton mirror, p_C and τ_C are p and τ of the Coude mirror. Our tolerances of p_N, τ_N, p_C, and τ_C are derived in the same manner as Ichimoto et al.[10] as 0.04, 0.3°, 0.04, and 0.3°, respectively.

Figure 3. A picture of a remotely controllable turret accommodating linear polarization attached at the entrance window of DST.

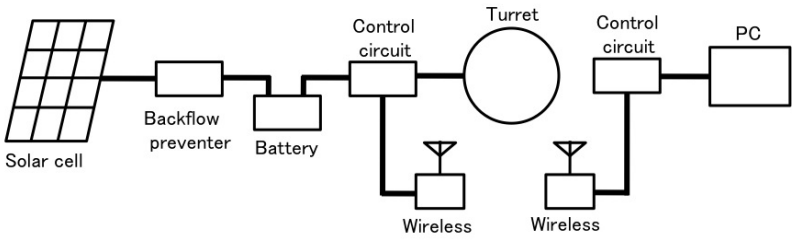

Figure 4. System diagram of the remotely controllable turret.

3.2 A remotely controllable turret accommodating polarizer

To measure the Mueller matrix of DST, we need to measure polarizations transformed by DST from well-known different incident polarizations. We are able to derive five unknown parameters (p_N, τ_N, p_C, τ_C, s) of our DST model by introducing unpolarized light and linear polarizations in different orientations from the entrance window.

We developed a turret accommodating linear polarizers, which can be remotely controled from the observation room. The machine is composed of two panels in rotation symmetry (Fig. 3). One works as the mask with fixed 8 holes and the other is a remotely controllable turret with 16 holes. The controllable turret accommodates 8 linear polarizers on every other hole with the same direction of the polarization axis and stops at 16 positions in 22.5° interval. When liner polarizers are under the mask hole, linearly polarized solar light enter the entrance window and when clear holes without polarizer are under the mask holes, solar light enter the window directly. The linear polarizers (Versalight, manufactured by Meadowlark Co.) constructed of a thin layer of Aluminum micro wires work as linear polarizer for wide wavelength range in visible and infrared.

Because of no pathway from observation room to the turret, we set a control circuit developed by a multipurpose Programmable Logic Controller on the controllable turret and control through transmission by 400 MHz radio waves from a PC in the observation room (Fig 4). An Absorbed Glass Mat battery set on the turret supplies the power and a solar cell auxiliary charges the battery to reduce the weight of the battery. The efficiency of our power system is quite high, because the solar cell always faces to the sun.

Requirements on the accuracy of the polarization angle and the side-runout of the turret are 0.5° and ±1°, respectively. A stepping motor and reduction gears control the turret with a resolution of 0.003° and the backlash produced by gears is 0.001°. By the driving system and a sensor of origin of the rotating turret, the error of polarization angle is constantly smaller than that of the requirement on the angle accuracy. Measured side-runout of the turret is less than ±0.006°.

Table 1. Information of observations

Date	Wavelength (nm)	Waveplate	Telescope position	Fitting residual*
2011. 4.17	630	quartz	east	0.007
2011. 4.17	656	quartz	east	0.013
2011. 4.17	854	quartz	east	0.014
2011. 4.17	630	quartz	west	0.011
2011. 4.17	656	quartz	west	0.009
2011. 4.17	854	quartz	west	0.007
2011. 9. 6	589	APSAW	east	0.040
2011. 9. 6	630	APSAW	east	0.013
2011. 9. 6	656	APSAW	east	0.016
2011. 9. 6	854	APSAW	east	0.014
2011. 9. 6	1083	APSAW	east	0.009
2012. 4.29	1083	quartz	west	0.020

* Root mean square of differences between the fitting results and the averages of Q/I, U/I, and V/I over the detector pixels are written.

3.3 Calibration of instrumental polarization of DST

The remotely controllable turret accommodating linear polarizers is attached at the entrance window of the telescope to induce a well known polarized light (solar light, $I = Q$, $I = -Q$, $I = U$, or $I = -U$) into the telescope and we observed continuum light of a quiet region at the solar disk center for the whole day. The continuum light is an ideal unpolarized light source whose polarization degree is $< 10^{-6}$ [19]. Table 1 show the list of calibration runs.

We developed the Mueller matrix model of DST to fit the observed data by Levenberg-Marquardt least-squares minimization method. Fitting parameters are five unknowns of the DST polarization model (p_N, τ_N, p_C, τ_C, s) and an angle offset of the origin of the remotely controllable turret. Figure 5 shows the one of results of fitting and Figure 6 is the obtained parameters (p_N, τ_N, p_C, τ_C, s) as function of the wavelength. DST produces the instrumental polarization if an ideal unpolarized light enters the entrance window of DST, and transform the polarization when a linear polarized light enter the window. Though observed instrumental polarization depends on the atitude of DST and inclination of the spectrograph slit, the Mueller matrix model of DST can reproduce the polarization well by tuning the 6 parameters with satisfactory small residuals of fitting as shown in Table 1.

The value of p_N, τ_N, p_C, and τ_C vary with the wavelength and the stray light s is a few par cent (Fig. 6). There are differences between these values when the telescope tube is set westward and eastward to the rotation axis of the azimuth. The origin angle of the remotely controllable turret changes with the observing day but the standard deviation of the angle is less than 0.2° on each day.

4. DISCUSSION AND SUMMARY

In order to open a new window of plasma diagnostics by using Zeeman effect, Hanle effect, Stark effect and impact polarization, we developed a new spectropolarimeter on the Domeless Solar Telescope at Hida observatory. The polarimeter consists of a 60 cm aperture vacuum telescope, a high dispersion slit vacuum spectrograph, polarization modulator/analyzer composed of a rotating waveplate and Wollaston prisms, and a detector. With a quartz and a APSAW as the waveplate and CCD camera and infrared camera as the detector, the system enables us to observe in wide range of wavelength covering from 400 nm to 1100 nm. A photometric accuracy of 10^{-3} can be achieved in ∼30 s and ∼60 s in visible and near infrared, respectively.

Instrumental polarization of the telescope is modeled by a set of Mueller matrices, in which two oblique mirrors have actions on polarization but others are idealized. Unpolarized and linearly polarized lights are introduced into the telescope by using a remotely controllable turret attached at the entrance window, and

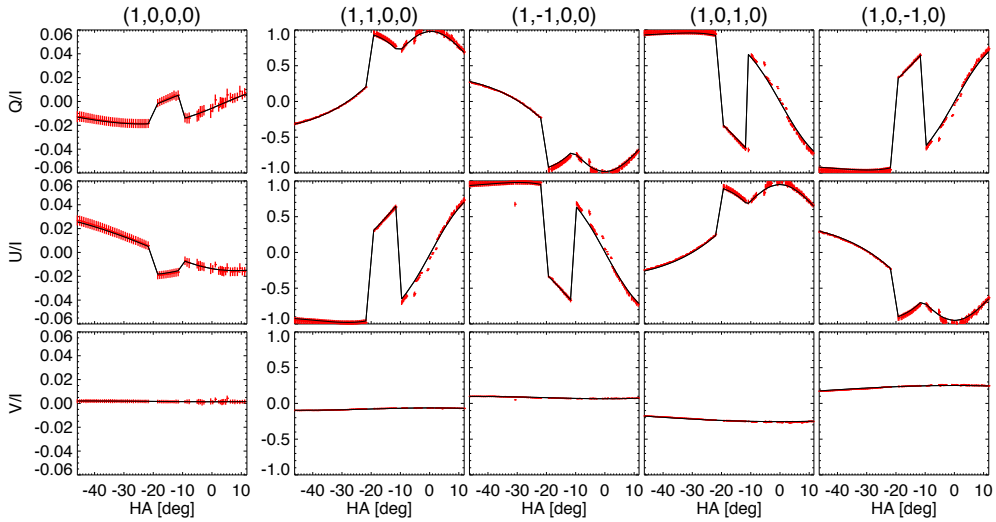

Figure 5. Products of the polarimeter (Q/I, U/I and V/I) for unpolarized and linearly polarized incident lights as a function of hour angle of the telescope. Data were taken in 1083 nm on 29 Apr. 2012. Red bars are for the observation data and the black curves are the fitting result with the DST model. The input Stokes vector to the DST is, as shown at the top of each column, unpolarized, $I = Q$, $I = -Q$, $I = U$, and, $I = -U$ from the left to the right. We change inclination angle of slit (θ_i) when hour angle is between -20° and -12°. The red bars scale the rms variation of each quantity over the detector.

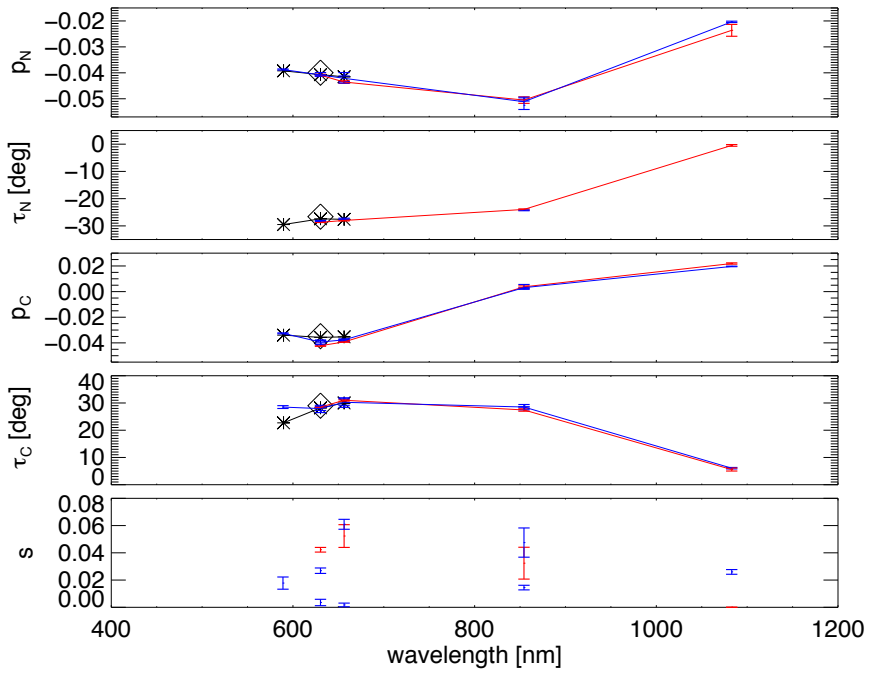

Figure 6. Variations of 5 parameters (p_N, τ_N, p_C, τ_C, and s) of our Mueller matrix telescope model against the wavelength. Red and blue plots are for the telescope tube in westward and eastward positions against the rotation axis of the azimuth, respectively. Error bars are standard deviations of the values along a spectrograph slit. Black line and asterisks are results of Hanaoka[17] and black diamond is the result of Kiyohara et al.[11] .

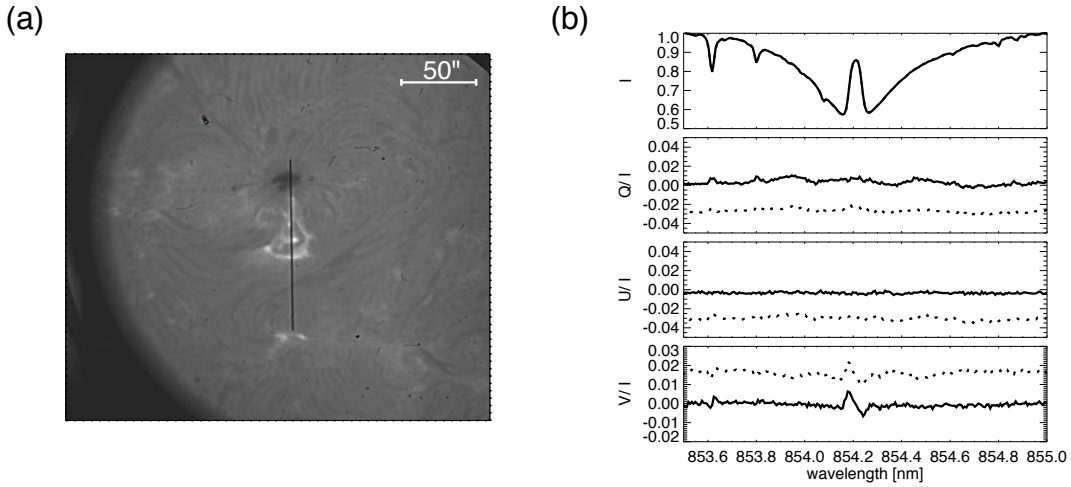

Figure 7. Stokes profiles of a flare kernel (b) taken with our polarimeter on 2011 April 18 in the Ca II 854 nm. Solid line and doted line are Stokes spectra after and before the calibration for the instrumental polarization, respectively. Left image (a) is slit-jaw image in Hα center. The black vertical line in the center of the left image is the spectrograph slit. The flare kernel is on the center of the slit.

observed responses of the polarimeter are fit with the Mueller matrix model by tuning 5 unknown parameters in the model. The fitting residuals are smaller than spatial variation of the observed Stokes vectors over the detector (Fig. 5) and smaller than the requirement on the scale error 0.05 (Table 1). In the small polarization degree regime, the residuals of instrumental polarization from our DST model are dominantly produced from the intensity. Since the variation of the instrumental polarization along the wavelength is negligible in the observing spectral window containing a few spectral lines, we can re-calibrate the Stokes profiles by using the polarization of the continuum. Stray light s produces a scale error in polarization magnitude. Spatial variation of s over the detector was found to be smaller than the requirement of 0.05.

In the model, the parameters of mirrors do not depend on the telescope tube position against the rotation axis of the azimuth, but our calibration show non-negligible difference between these values when the telescope tube is set westward and eastward to the rotation axis of the azimuth. The cause of the discrepancy is not identified yet. Our results are slightly different from previous works in 600 nm wavelength range (Fig. 6). The parameters of the mirrors might also change slowly due to aging of coatings, etc.. They are needed to be updated. It is possible to derive the 3 parameters (p_N, p_C, and τ_C) without the turret on the entrance window but with only the continuum light at the disk center. We plan to make such quick calibration in more frequent manner to monitor the aging effect or seasonal variations of these parameters.

Figure 7 shows an examples of observation data taken with our polarimeter. This is a Stokes spectrum of a flare kernel on 2011 April 18 in the Ca II 854 nm. We put the spectrograph slit on the flare kernel and we show their Stokes spectrum before and after calibration for the instrumental polarization. It took 19 s to obtain the spectrum and the spatial sampling and the resolution of the wavelength are 0.8 arcsec and 7 pm, respectively. The flare kernel makes the Ca II 854 nm line center emission and Zeeman effect appears in the Stokes-V profile.

ACKNOWLEDGMENTS

This work was supported by a Grant-in-Aid for Scientific Research (No. 22244013, P.I. K. Ichimoto) from the Ministry of Education, Culture, Sports, Science and Technology of Japan, and by the Grant-in-Aid for the Global COE Program "The Next Generation of Physics, Spun from University and Emergence" from the Ministry of Education, Culture, Sports, Science and Technology (MEXT) of Japan. The authors also thanks to Dr. R.

Kitai, Mr. N. Kaneda and staff member of Hida observatory for the continuous support in instrument setup and observations.

REFERENCES

[1] Hale, G. E., "On the probable existence of a magnetic field in sun-spots," *Astrophysical Jounal* **28**, 315–343 (1908).

[2] Gandorfer, A. M. and Povel, H. P., "First observations with a new imaging polarimeter," *Astronomy and Astrophysics* **328**, 381–389 (1997).

[3] Collados, M., Lagg, A., Garcí, A. J. J. D., Suárez, E. H., López, R. L., Mañá, E. P., and Solanki, S. K., "Tenerife infrared polarimeter ii," in [*The Physics of Chromospheric Plasmas ASP Conference Series*], Heinzel, P., Dorotovič, I., Rutten, R. J., and of the Pacific, S. F. A. S., eds., *Proc. of the conference held 9-13 October, 2006 at the University of Coimbra in Coimbra, Portugal*, 611–616 (2007).

[4] Jaeggli, S. A., Lin, H., Mickey, D. L., Kuhn, J. R., Hegwer, S. L., Rimmele, T. R., and Penn, M. J., "Firs: a new instrument for photospheric and chromospheric studies at the dst," *Memorie della Societa Astronomica Italiana* **81**, 763–768 (2010).

[5] Stenflo, J. O., "The hanle effect and the diagnostics of turbulent magnetic fields in the solar atmosphere," *Solar Physics* **80**, 209–226 (1982).

[6] Stenflo, J. O. and Keller, C. U., "The second solar spectrum. a new window for diagnostics of the sun," *Astronomy and Astrophysics* **321**, 927–934 (1997).

[7] Bueno, J. T., Degl'Innocenti, E. L., Collados, M., Merenda, L., and Sainz, R. M., "Selective absorption process as the origin of puzzling spectral line polarization from the sun," *Nature* **415**, 403–406 (2002).

[8] Foukal, P. and Hinata, S., "Electric fields in the solar atmosphere - a review," *Solar Physics* **132**, 307–334 (1991).

[9] Henoux, J. C., Chambe, G., Smith, D., Tamres, D., Feautrier, N., Rovira, M., and Sahal-Brechot, S., "Impact line linear polarization as a diagnostic of 100 kev proton acceleration in solar flares," *Astrophysical Journal Supplement Series* **73**, 303–311 (1990).

[10] Ichimoto, K., Lites, B., Elmore, D., Suematsu, Y., Tsuneta, S., Katsukawa, Y., Shimozu, T., Shine, R., Tarbell, T., Title, A., Kiyohara, J., Shinoda, K., Card, G., Lecinski, A., Streander, K., Nakagiri, M., Miyashita, M., Noguchi, M., Hoffmann, C., and Cruz, T., "Polarization calibration of the solar optical telescope onboard hinode," *Solar Physics* **249**, 233–261 (2008).

[11] Kiyohara, J., Ueno, S., Kitai, R., Kurokawa, H., Makaita, M., and Ichimoto, K., "Calibration of the instrumental polarization of the domeless solar telescope at the hida observatory," in [*Ground-based Instrumentation for Astronomy*], Moorwood, A. F. M. and Masanori, I., eds., *Proc. SPIE* **5492**, 1778–1785 (2004).

[12] Nakai, Y. and Hattori, A., "Domeless solar tower telescope at the hida observatory," *Kyoto University, Faculty of Science, Memoirs, Series of Physics, Astrophysics, Geophysics and Chemistry* **36**, 385–399 (1985).

[13] del Toro Iniesta, J. and Collados, M., "Optimum modulation and demodulation matrices for solar polarimeter," *Applied Optics* **39**, 1637–1642 (2000).

[14] Ichimoto, K., Shinoda, K., Yamamoto, T., and Kiyohara, J., "Photopolarimetric measurement system of mueller matrix with dual rotating waveplates," *Publications of the National Astronomical Observatory of Japan* **9**, 11–19 (2006).

[15] Nakai, Y., "New domeless solar telescope in hida observatory," in [*Japan-France Seminar on Solar Physics*], Moriyama, F. and Henoux, J. C., eds., *Proc. teh Conference*, 275 (1980).

[16] Makita, M., Funakoshi, Y., and Hanaoka, Y., "Polarization of the domeless solar telescope of the hida observatory (preliminary report)," in [*Solar Polarimetry*], L. J. November. Sunspot, N., ed., *Proc. the 11th Sacramento Peak Summer Workshop*, 198–210 (1991).

[17] Hanaoka, Y., "Spectropolarimetry with the hida domeless solar telescope," *Publications of the Astronomical Society of Japan* **61**, 357–365 (2009).

[18] Skumanich, A., Lites, B. W., Pillet, V. M., and Seagraves, P., "The calibration of the advanced stokes polarimeter," *Astrophysical Jounal Supplement* **110**, 357–380 (1997).

[19] Stenflo, J. O., "Polarization of the sun's continuous spectrum," *Astronomy and Astrophysics* **429**, 713–730 (2005).